nature communications

Article

https://doi.org/10.1038/s41467-025-62378-6

Crosstalk between inovirus core gene and accessory toxin-antitoxin system mediates polylysogeny

Received: 18 December 2024

Accepted: 15 July 2025

Published online: 07 August 2025

Check for updates

Jiayu Gu[1,2], Yunxue Guo[1,2], Juehua Weng[1,2], Shituan Lin[1,2], Yabo Liu[1] & Xiaoxue Wang[1,2]

Polylysogeny, the harboring of multiple prophages within a single bacterial genome, is common among bacterial pathogens and enhances virulence and genome plasticity. Inoviruses (filamentous phages) are often present in multiple copies in major pathogens, leading to polylysogeny. Two highly similar filamentous phages (Pf4 and Pf6) are integrated into the widely distributed model *Pseudomonas aeruginosa* strain, and both prophages are activated during biofilm formation. It remains unclear whether the two prophages function competitively or cooperatively. Here, we show a crosstalk between Pf4's core region protein RepG4 (PA0717) and Pf6's accessory KKP (kinase-kinase-phosphatase) toxin-antitoxin module that coordinates their propagation. RepG4, involved in Pf4 phage replication, triggers kinase-mediated toxicity of KKP in a dose-dependent manner by degrading the phosphatase antitoxin. This crosstalk serves as a molecular brake, preventing excessive Pf4 production and coordinating the release of both Pf4 and Pf6 phages during biofilm maturation. Our findings provide valuable insights into the significance of the tight regulation between phage core genes and accessory genes in establishing a mutualistic interaction between co-resident prophages.

Bacteriophages and their hosts are engaged in a predator–prey relationship. Temperate phages can either remain quiescent as prophages, replicating synchronously with the host chromosome, or enter a lytic cycle, producing virions[1]. Previous analysis revealed that pathogens, including *Escherichia coli*[2,3], *Salmonella*[4,5], *Pseudomonas*[6], and *Listeria*[7], often carry multiple prophages, resulting in polylysogeny[8,9]. The diversity of prophages often encodes the evolutionary history of the pathogen and reflects its adaptability to the promiscuous lifestyle[9]. When a single prophage is activated under stress or specific environmental conditions, it can modulate the activity of coexisting prophages, either inducing their excision or suppressing their expression[4,10,11]. The lysogeny-lysis conversion of prophage is commonly regulated by the phage repressor and antirepressor[12,13]. Previous work demonstrated that anti-repressors can act on non-cognate repressors, providing the basis for a crosstalk that allows coordinating the induction of multiple prophages in polylysogenic *Salmonella*[4]. Another regulatory module in inter-prophage competition involves a transcription factor that directs a small protein to inactivate the prophage repressor, leading to the specific activation of its own prophage[14].

Inoviruses, or filamentous phages, are widespread in various environments and infect a diverse range of bacterial hosts, including *Vibrio cholera*[15,16] and *Pseudomonas aeruginosa*[15,17]. Comparative genomics revealed high inovirus prevalence in major pathogens and these viruses are often present in multiple copies within the same host cells[15,18,19]. Unlike temperate phages such as Lambda, which typically trigger rapid host lysis upon activation, inoviruses establish a chronic infection, persistently releasing viral progeny through a non-lytic "budding" mechanism[15]. It remains unclear whether co-resident filamentous prophages function competitively or cooperatively during prophage activation in pathogens.

[1]State Key Laboratory of Tropical Oceanography, South China Sea Institute of Oceanology, Chinese Academy of Sciences, Guangzhou, China. [2]University of Chinese Academy of Sciences, Beijing, China. e-mail: xxwang@scsio.ac.cn

Each prophage carries unique accessory genes, contributing to the mosaic nature of bacterial genomes[18]. Variations in genetic content, integration sites, and life cycle strategies enable prophages to perform specialized functions across diverse bacterial hosts, influencing a wide array of phenotypic traits[20]. For instance, prophage-encoded virulence factors facilitate bacterial colonization and survival[1,21]. Prophages serve as reservoirs for various defense systems and anti-defense systems, including restriction modification systems[22,23], toxin-antitoxin (TA) systems[24–26] and anti-CRISPRs[20,27]. Over the past few decades, several strategies have emerged that these prophage-encoded defense systems use to specifically target lytic phage infections by attacking phage structural proteins[28,29], replication proteins[6], and even inactivating phage receptors on host cell surfaces to block adsorption[30]. In cases of polylysogeny, co-residing prophages can shift their interactions from competition to mutualism in response to external stressors, working together to combat invaders[22]. However, the functioning of these prophage-encoded defense systems during prophage induction in polylysogenic pathogens remains largely unexplored.

In two sublines of *P. aeruginosa*, one strain (designed as PAO1) contains only the Pf4 prophage, while a closely related strain (designed

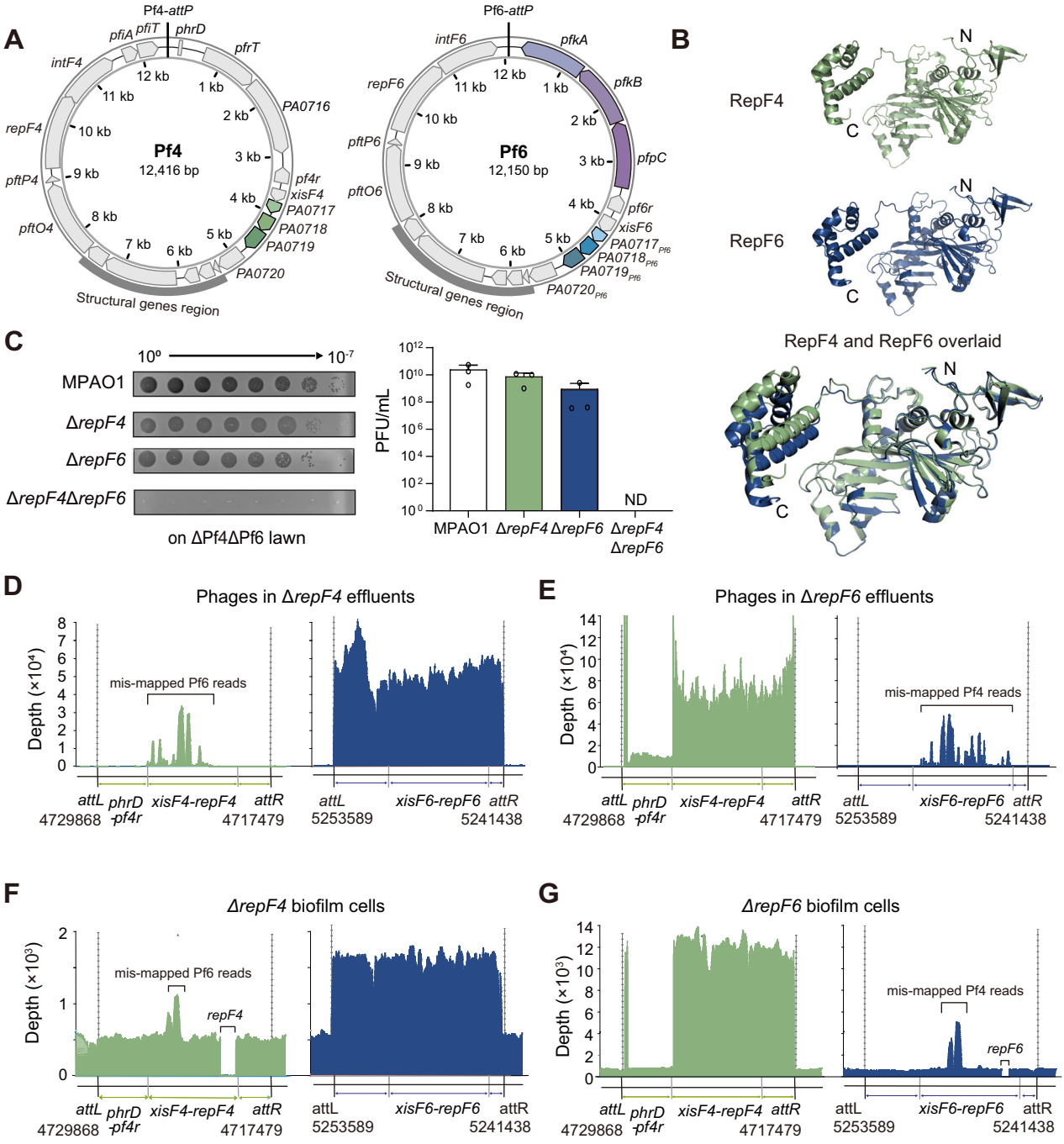

Fig. 1 | RepF4 controls Pf4 and RepF6 controls Pf6 prophage genome replication. A Annotation of Pf4 and Pf6 prophage genomes in MPAO1. *PA0717-PA0718-PA0719* in Pf4 and Pf6 were shown in green and blue, respectively. KKP were shown in purple. **B** The overlay of RepF4 structure (green) and RepF6 structure (blue) predicted by AlphaFold Protein Structure Database. **C** Phages were collected from biofilm effluents on Day 6. Serial dilutions were applied to lawns of ΔPf4ΔPf6 and PFUs were calculated. Three independent cultures were used in C, and data were shown as mean ± SD. One-way ANOVA was used for comparisons with 95% confidence intervals. No statistically significant difference was observed. Genome sequencing of phages in the biofilm effluents of Δ*repF4* (**D**) or Δ*repF6* (**E**) on day 6. Genome sequencing of biofilm cells of Δ*repF4* (**F**) or Δ*repF6* (**G**) on day 6. Source data are provided as a Source Data file.

as MPAO1) carries an additional Pf prophage, Pf6[31,32]. Importantly, both Pf prophages are activated during biofilm formation of MPAO1[6]. These Pf phages play critical roles in mediating biofilm formation and virulence in the lung[6,17,33–35], and can also suppress mammalian immunity by directly inhibiting phagocytosis and bacterial clearance[36]. Therefore, the integration of Pf prophages and the activation of Pf phages during biofilm development are critical for the pathogenic lifestyle of *P. aeruginosa*.

The genomes of inoviruses are relatively small (<15 kb) and comprise a conserved core genome alongside a diverse accessory genome[15]. The accessory genomes of inoviruses are enriched with various defense genes, particularly TA systems[15]. Notably, Pf4 and Pf6 exhibited a strikingly high degree of similarity in their core genomic regions (>98% nucleotide identity), while diverging primarily in their accessory TA genes[6]. In the accessory genome of Pf4 prophage, the toxin PfiT and its upstream antitoxin PfiA form a type II TA pair, and the deletion of *pfiT* stimulates the production of Pf4[37]. Another cluster in the accessory genome of Pf4 prophage contains a non-coding RNA, PhrD, and a reverse transcriptase PfrT that edits the Pf4 phage genome, facilitating the generation of superinfective (SI) form Pf4 under biofilm conditions[38]. In the accessory genome of Pf6 prophage, a kinase-kinase-phosphatase (KKP) TA system regulates prophage activation via phosphorylating host silencer MvaU and also provides defense against lytic phage infection[6]. Interestingly, the virus-to-host ratio was consistently maintained at ~2:1, regardless of the presence of one or both prophages in the host cells[6]. These findings suggest that Pf4 and Pf6 establish a mutualistic relationship with their host. However, it remains unclear whether the two sister prophages function competitively or cooperatively during Pf activation.

In this study, we investigated crosstalk between Pf4 and Pf6 prophages, focusing on phage proteins in the core region and regulatory elements. Contrary to expectations of dedicated crosstalk between repressor and anti-repressor or replication initiation proteins, we discovered that a Pf4 core region protein RepG4 (PA0717) triggers KKP TA module toxicity in Pf6. This occurs via degradation of the antitoxin PfpC of KKP, releasing the toxicity of PfkA and PfkB. This crosstalk coordinates the release of both phages during biofilm formation, contributing to the maintenance of polylysogeny and pathogenicity.

Results

Crosstalk between the replication initiator proteins of the two prophages

The MPAO1 strain studied here was obtained from C. Manoil lab at the University of Washington in 2007, a lineage of PAO1 that has been utilized to create a widely used transposon mutant bank[31]. The core genome region of Pf prophage is 8–9 kb. Pf4 and Pf6 share a highly similar core region (*PA0717-repF*, with over 98% nucleotide identity) (Fig. 1A; Table 1), encoding a ssDNA binding protein PA0720, five structural proteins (PA0721-PA0725), a *zot*-like assembly-export protein PA0726, a toxic polypeptide PA0726.1 and a rolling cycle replication initiator protein RepF. The minor capsid protein pVII allows exclusion of SI-Pf phages by interfering with type IV pilus (T4P) function, and minor capsid proteins pIII and pVII provide host protection against infection by several pilus-dependent lytic phages[39,40].

To investigate the interaction between Pf4 and Pf6, we first examined potential crosstalk between their respective rolling circle replication (RCR) initiator proteins. Sequence alignment and predicted structural modeling revealed high similarity between RepF4 (from Pf4) and RepF6 (from Pf6), with 95.3% amino acid identity (Fig. 1B; Supplementary Fig. 1). Both proteins contain two conserved motifs essential for RCR: a metal-ion-binding HUH motif (His-hydrophobic-His) and a catalytic YxxxY motif (containing two conserved tyrosines)[41,42] (Supplementary Fig. 1).

Since both phages were produced and released during biofilm development[6], we investigated whether these co-resident prophages could utilize non-cognate RepF proteins for replication. We generated mutant strains (Δ*repF4*, Δ*repF6*, and Δ*repF4*Δ*repF6*) with partial deletions of the *repF* genes (encoding RepF proteins) in each prophage, while preserving the flanking *intF* integrase genes. Phage production was monitored in a flow-cell biofilm model using plaque assays on biofilm effluents. To assess superinfection, we performed plaque assays using a wide-type MPAO1 strain and a ΔPf4ΔPf6 strain lacking both prophages. Finally, qPCR using prophage-specific primers quantified the relative abundances of Pf4 and Pf6 phages in the biofilm effluents.

Deletion of either *repF4* or *repF6* did not affect biofilm phage production; however, deleting both genes completely abolished it (Fig. 1C and Supplementary Fig. 2A). Whole-genome sequencing of phage DNA (day 6, using a custom single-stranded DNA sequencing method) revealed that only Pf4 phage was produced in Δ*repF6* biofilms, and only Pf6 phage in Δ*repF4* biofilms (Fig. 1D, E), demonstrating a lack of RepF protein crosstalk in phage replication. This was further confirmed by the observation that only Pf4 and Pf6 genes, respectively, were replicated in the corresponding mutant biofilms (Fig. 1F, G and Supplementary Fig. 2B, C). Therefore, each Pf prophage's RepF protein is dedicated to its own genome replication.

Phage repressors and antirepressors inhibit activation of their cognate prophages

We next investigated potential crosstalk between phage antirepressors and non-cognate repressors, a mechanism that often coordinates prophage induction in polylysogens[3]. Pf4 and Pf6 each possess their own repressor/antirepressor pair. Pf4r and Pf6r exhibit moderate amino acid sequence similarity (51% identity; Supplementary Fig. 3A) and high structural similarity (Fig. 2A). Phage production in planktonic cultures of Δ*pf4r* and Δ*pf6r* mutant strains was assessed. Deletion of either *pf4r* or *pf6r* resulted in phage production (Fig. 2B), predominantly Pf4 phage in Δ*pf4r* and exclusively Pf6 phage in Δ*pf6r* cells (Fig. 2B).

Our previous work demonstrated that XisF4 functions as both an excisionase and activator in the Pf4 lifecycle[13]. A putative ORF (XisF6) was identified in Pf6 at a similar genomic location but in the opposite orientation to *pf6r*, exhibiting low similarity to XisF4 (Fig. 2C and Supplementary Fig. 3B). Consistent with our previous findings, *xisF4* overexpression (using pHERD20T-*xisF4*) in planktonic MPAO1 cells resulted in abundant Pf4 phage production (Fig. 2D). In contrast, *xisF6* overexpression did not produce detectable phage virions (plaque assay) nor activate *intF6* (Fig. 2D). To assess the impact of XisF on Pf prophage genome excision and phage propagation during MPAO1 biofilm formation, we quantified the frequency of prophage excision (*attB/gyrB*) and the copy number of RF of Pf (*attP/gyrB*) following XisF overproduction. Consistent with previously reported[13], XisF4 induced Pf4 prophage excision, significantly increasing the levels of circularized RF-Pf4 (Fig. 2D). In contrast, XisF6 failed to induce Pf6 excision, and no circularized Pf6 was detected upon overexpression of XisF6 (Fig. 2D). Intriguingly, unlike Pf4 phages that predominantly package circularized ssDNA genomes as either full-length (non-SI Pf4) or reduced forms (SI Pf4), only a minimal amount of the circularized Pf6 genome (~0.01%) was detected in Pf6 phages released in day 6 biofilm cells (Supplementary Fig. 3C, D). These findings suggest that Pf6 may employ a replication strategy distinct from that of Pf4 during biofilm development.

PA0717 of Pf4 (RepG4) in the core genome participates in the synthesis of RF Pf4

The Pf core genome is conserved across both plasmid-like Pf1 phage (in the PAK strain) and integrated prophages, including Pf5 (in the PA14 strain), Pf4 and Pf6. In these prophages, the genes *PA0717*, *PA0718*, and *PA0719* are situated between the phage antirepressor XisF and the single-stranded DNA-binding protein PA0720, maintaining consistent genomic organization (Supplementary Fig. 4A). Sequence analysis demonstrated high amino acid similarity of PA0717, PA0718,

Table 1 | Pf filamentous phage genes and relative function and interaction network

Pf4 locus tag (MPAO1)	Gene ID in Pf4	Gene name in Pf4	Pf6 locus tag (MPAO1)	Gene name in Pf6	Product/Function	Regulation/ interaction	References
MP_4506	PA0714.1	*phrD*			non-coding RNA	RhlR	38,60
MP_4505	PA0715	*pfrT*			reverse transcriptase involves in the synthesis of SI Pf4 genome		38
MP_4504	PA0716				an ATPase with AAA domain		38
			MP_4992	*pfkA*	serine/threonine kinase, together with *pfkB* function as the toxin of KKP TA system	MvaU	6
			MP_4991	*pfkB*	serine/threonine kinase, together with *pfkA* function as the toxin of KKP TA system	MvaU	6
			MP_4990	*pfpC*	serine/threonine phosphatase, anti-toxin of KKP TA system		6
MP_4503	PA0716.1	*pf4r*	MP_4989	*pf6r*	repressor, maintenance of lysogeny	LasB, OxyR	12,19,61
MP_4502	PA0716.2	*xisF4*	MP_4988	*xisF6*	excisionase and prophage activator		13
MP_4501	**PA0717**	***repG4***	**MP_4987**	***repG6***	unknown		this study
MP_4500	**PA0718**	***pflM***	**MP_4986**	***pflM***	lysogeny maintenance		43
MP_4499	**PA0719**		**MP_4985**		unknown		
MP_4498	**PA0720**		**MP_4984**		single-strand DNA binding protein		
MP_4497	**PA0721**	***pfsE(gVII)***	**MP_4983**	***pfsE(gVII)***	minor capsid protein, superinfection exclusion	PilC, PilJ, PqsA	39,40,62
MP_4496	**PA0722**	***gIX***	**MP_4982**	***gIX***	minor capsid protein		
MP_4495	**PA0723**	***gVIII***	**MP_4981**	***gVIII***	major capsid protein		
MP_4494	**PA0724**	***gIII***	**MP_4980**	***gIII***	minor capsid protein	PilJ, TolR, TolA	39
MP_4493	**PA0725**	***gVI***	**MP_4979**	***gVI***	minor capsid protein		
MP_4492	**PA0726**	***pftO4***	**MP_4978**	***pftO6***	phage zot-like assembly-export protein		45
MP_4491	**PA0726.1**	***pftP4***	**MP_4977**	***pftP6***	unknown		45
MP_4490	**PA0727**	***repF4***	**MP_4976**	***repF6***	replication initiator protein	UvrD, HU	6,46
MP_4489	PA0728	*intF4*	MP_4975	*intF6*	integrase		
MP_4488	PA0728. 1	*pfiA*			antitoxin of PfiTA TA system		37
MP_4487	PA0729	*pfiT*			inhibition of Pf4, toxin of PfiTA TA system		37

The core region of Pf4 and Pf6 is highlighted in bold format.

and PA0719 among Pf phages (Supplementary Fig. 4B), with PA0718 recently characterized as a lysogeny maintenance protein (renamed PflM)[43]. PA0719 exhibits a conserved N-terminal domain but displays divergent C-terminal regions among the prophages (Supplementary Fig. 4B), suggesting potential functional or regulatory diversification.

We leveraged transcriptomic data from our prior study[6] and found that these three genes (*PA0717-PA0718-PA0719*) are significantly induced in biofilm cells and exhibit the highest expression levels among the Pf4 genes[6], while they remain silent in the planktonic state when the Pf4 prophage is in a quiescent condition (Fig. 3A). To explore the functions of these three genes, we constructed single gene deletion as well as multiple-gene deletion mutants, followed by tests on phage production. Our findings revealed that deleting *PA0717* or the combined deletion of *PA0717*, *PA0718*, and *PA0719* (Δ171819) reduced Pf phage production in biofilms (Fig. 3B, C). Recent studies demonstrated that non-SI Pf4 phage production in early biofilm development results from the de-repression of *xisF4*, a process mediated by KKP-dependent dephosphorylation of MvaU[38]. Notably, the deletion of *PA0717* predominantly diminished the production of non-SI Pf4 phages generated during the early stages of flow-cell biofilm formation (<day 5) (Fig. 3B, C).

To determine whether PA0717 contributes to non-SI Pf4 phage production, we overexpressed *xisF4* in planktonically cultured MPAO1 strains. As previously reported[13], *xisF4* overexpression triggered formation of the replicative form (RF) Pf4, leading to non-SI Pf4 production with intact phage genomes. Consistent with prior findings, deletion of *repF4* abolished XisF4-mediated Pf4 activation (Fig. 3D). Remarkably, PA0717 deletion alone eliminated RF Pf4 production (Fig. 3D–F), suggesting that PA0717 is likely involved in Pf4 prophage genome replication. To exclude potential crosstalk with Pf6, we repeated experiments in a Pf6 prophage-deficient PAO1 strain, and same results were obtained (Supplementary Fig. 5). In contrast, deletions of PA0718 or PA0719 had no effect on RF Pf4 synthesis. Based on its potentially functional role, we propose renaming PA0717 as RepG, with RepG4 (Pf4-derived) and RepG6 (Pf6-derived) denoting its prophage-specific isoforms. Intriguingly, RepG homologs across four Pf phages share a conserved arginine-enriched motif (14–15 of 70 residues) in their C-terminal domains (Supplementary Fig. 4B), a biochemical signature strongly associated with DNA-protein interaction and transcriptional regulation[44]. The conserved arginine-enriched motif underscores RepG's potentially critical role in Pf phage replication.

RepG4 activates the kinase-based toxicity of the KKP TA system

In our recent study, we demonstrated that the KKP module of Pf6 can defend against infections by several lytic phages by activating the kinase-based toxicity[6]. Specifically, KKP modules provide protection against the *E. coli* lytic phage T4 by targeting the phage helicase loader Gp59 protein[6]. The Pf phages released during biofilm development can re-infect the host cells to cause cell death, we then tested whether KKP can defend the re-infection of the Pf phages. Pf4 and Pf6 phages in the biofilm effluents of the Δ*repF6* and Δ*repF4* strains were collected for the plaque assays. Overexpression of the KKP module conferred

https://doi.org/10.1038/s41467-025-62378-6

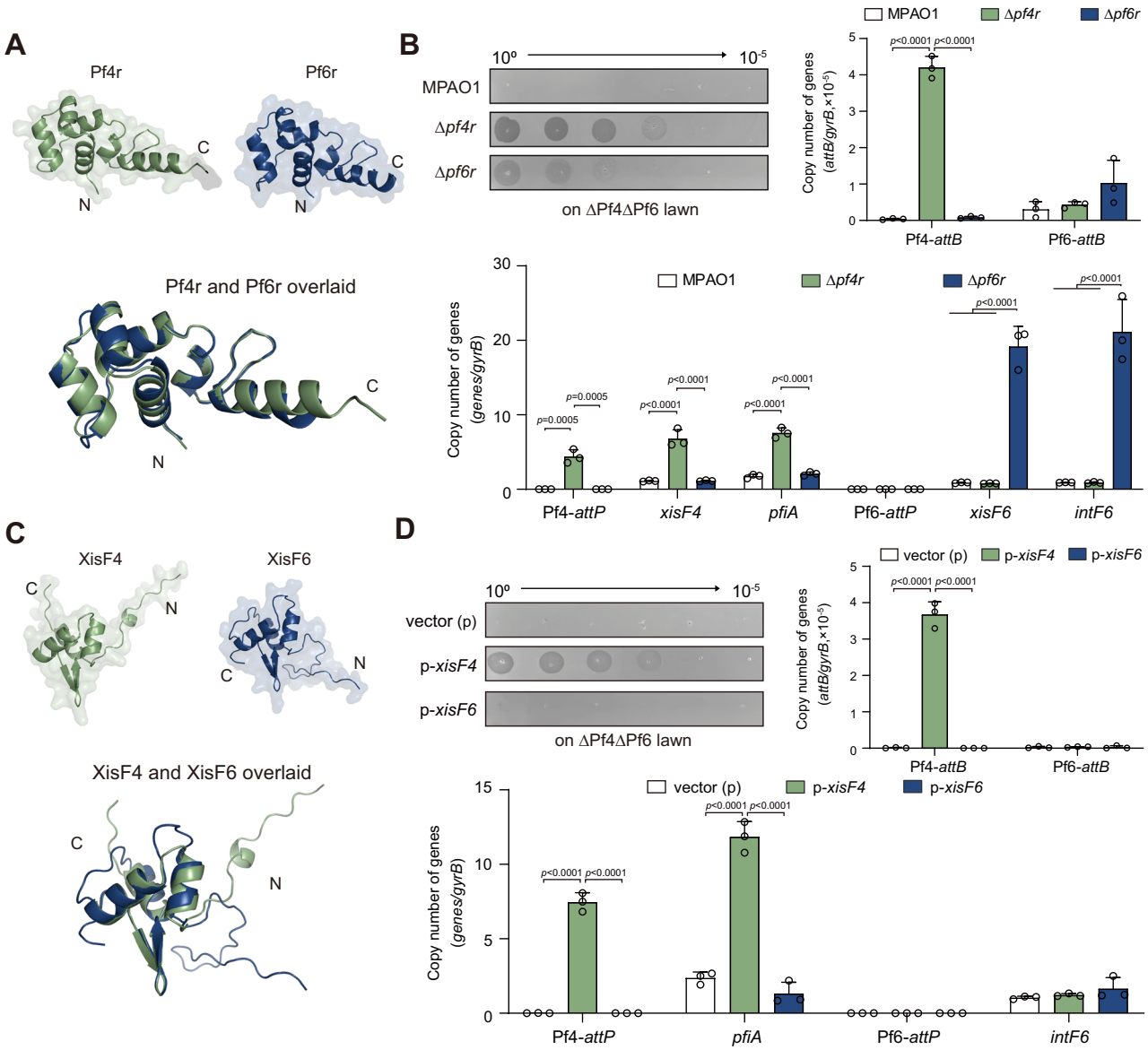

Fig. 2 | Phage repressors and antirepressors specifically inhibit activation of their cognate prophages. A The overlay of the predicted structures of Pf4r (green) and Pf6r (cyan) structures. **B** Phage titers of planktonic supernatant from MPAO1, Δ*pf4r* and Δ*pf6r* (upper left lane). Copy numbers of Pf4-*attB* and Pf6-*attB* (upper right lane), Pf4-*attP*, Pf6-*attP*, indicated Pf4 genes and indicated Pf6 genes (lower lane) were determined. **C** Overlay of the predicted XisF4 structure (green) and the XisF6 structure (cyan). **D** Phage titers of planktonic supernatant from MPAO1 carrying pHERD20T (vector(p)), pHERD20T-*xisF4* (p-*xisF4*) and pHERD20T-*xisF6* (p-*xisF6*) (upper left lane). Copy numbers of Pf4-*attB* and Pf6-*attB* (upper right lane), Pf4-*attP*, Pf6-*attP*, indicated Pf4 gene and indicated Pf6 gene (lower lane) were determined. Three independent cultures were used, and data were shown as mean ± SD. Two-way ANOVA was used for comparisons with 95% confidence intervals. $p < 0.05$ was considered statistically significant. Source data are provided as a Source Data file.

resistance against both Pf phages, though the observed protection resulted in only a modest 2 to 3 log reduction in phage titers (Fig. 4A). This limited reduction may reflect the inherently attenuated plaque-forming efficiency of Pf phages compared to canonical lytic phages.

Each of the thirteen Pf4 core genes was co-expressed with the KKP module using a two-plasmid system induced by IPTG and *L*-arabinose, respectively. Six of them (*PA0719*, *PA0721*, *PA0723*, *PA0724*, *PA0726*, and *PA0726.1*) performed strong toxicity alone, including four membrane-anchored genes (*PA0721*, *PA0723*, *PA0724*, and *PA0726.1*)[39,45], a *zot*-like assembly-export gene *PA0726* and an unknown function gene *PA0719* (Fig. 4B; Supplementary Fig. 6A). Those proteins are incorporated into virions during assembly and release; therefore, they do not accumulate to high levels. However, we found that only *repG4* activated KKP-mediated toxicity, while being slightly toxic when overexpressed alone in planktonic cells (Fig. 4B; Supplementary Fig. 6B). Importantly, co-expression of *repG4* with $K^{GFI}KP$[6] (containing an inactive kinase with a mutated GFI motif) was less toxic than that co-expressed with KKP (Fig. 4C; Supplementary Fig. 6C). Critically, in vitro phosphatase assays revealed that increasing molar ratios of RepG4 to PfpC suppressed PfpC enzymatic activity (Fig. 4D; Supplementary Fig. 7A, B). Pull-down assays confirmed direct interaction between His-tagged RepG4 and Flag-tagged PfpC (Fig. 4E Supplementary Fig. 7C). This mechanism positions RepG4 as a molecular switch regulating KKP-mediated host stress during phage induction.

RepG4 triggers the degradation of PfpC antitoxin during Pf4 activation

Given the inherent instability typical of antitoxin components in TA systems, we investigated whether Pf phage infection induces PfpC

https://doi.org/10.1038/s41467-025-62378-6

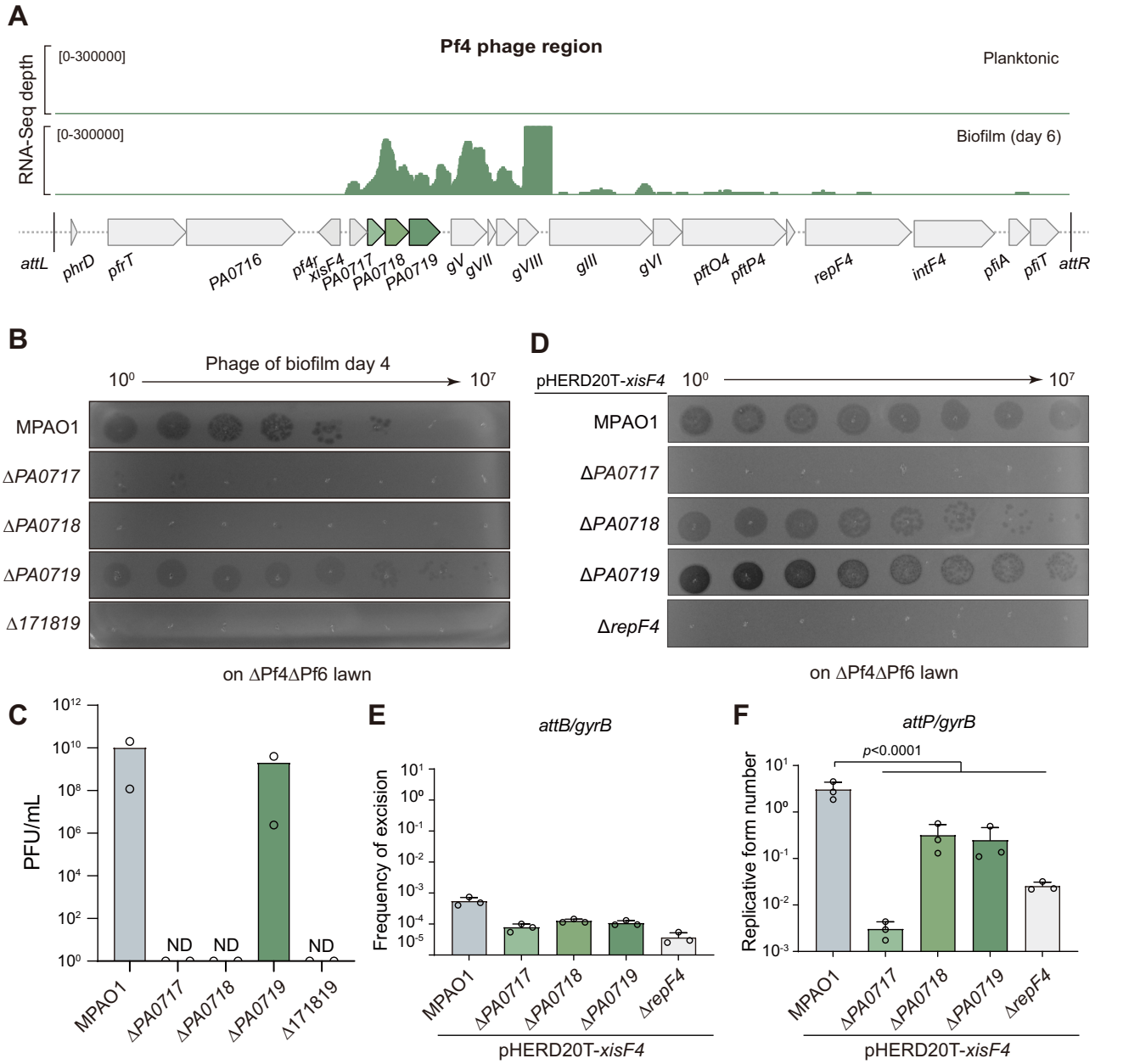

Fig. 3 | RepG4 (PA0717 of Pf4) participates in the synthesis of RF Pf4. A RNA-seq read coverage of Pf4 transcripts in MPAO1 biofilm and planktonic cells (the transcriptomic data presented here were derived from the same dataset as that used in our previously published work[6]). **B** Phage titers of biofilm effluents from 4-day biofilms of MPAO1, Δ*PA0717*, Δ*PA0718*, Δ*PA0719*, and Δ*171819*. **C** Phage titers in (**B**) were calculated. Two independent cultures were used. **D** Phage titers of planktonic effluents from MPAO1, Δ*PA0717*, Δ*PA0718*, Δ*PA0719*, and Δ*repF4* carrying pHERD20T-*xisF4*. **E** The frequency of Pf4 excision in (**D**) was quantified. **F** The numbers of RF Pf4 molecules in (**D**) were quantified. Three independent cultures were used in (**E**) and (**F**), representative images were shown in (**D**). Data in (**E**) and (**F**) were shown as mean ± SD. Two-way ANOVA was used for comparisons with 95% confidence intervals. $p < 0.05$ was considered statistically significant. Source data are provided as a Source Data file.

degradation to liberate the toxic activity of PfkA and PfkB. Purified C-terminal His-tagged PfpC migrated as two distinct bands on SDS-PAGE (Supplementary Fig. 8A). N-terminal sequencing and western blotting identified these bands as full-length PfpC (~41 kDa) and a stable fragment, PfpC^{SFc} (~35 kDa), lacking ~44 C-terminal amino acids that encompass a predicted disordered region[6] (Supplementary Fig. 8B). Both isoforms remained stable over time at 4 °C in the presence of MPAO1 lysate (Supplementary Fig. 8A). Notably, we previously demonstrated that C-terminally degraded PfpC retained its ability to neutralize PfkA-PfkB toxicity when co-expressed with the kinases[6]. To probe PfpC degradation dynamics, we incubated purified C-terminal His-tagged PfpC with lysates from planktonically grown MPAO1, Δ*pf4r*, and Δ*pf6r* strains. Western blot analysis revealed gradual PfpC degradation in MPAO1 lysate at 37 °C over time (Fig. 5A). Interestingly, the degradation was accelerated in Δ*pf4r* lysate while suppressed in Δ*pf6r* lysate, implicating Pf4- and Pf6-derived factors have different roles in PfpC stability (Fig. 5A and Supplementary Fig. 8C).

Despite high sequence conservation in the Pf4 and Pf6 core gene regions, we identified a notable 6-bp difference (5′-ATGCGC-3′) encompassing the *repG4* start codon (ATG) that is absent in *repG6* (Fig. 5B). Instead, both *repG* genes share an upstream GTG codon preceded by putative ribosome binding sites (RBS) and we hypothesized that *repG6* may use this GTG as the start codon (Fig. 5B). To verify

https://doi.org/10.1038/s41467-025-62378-6

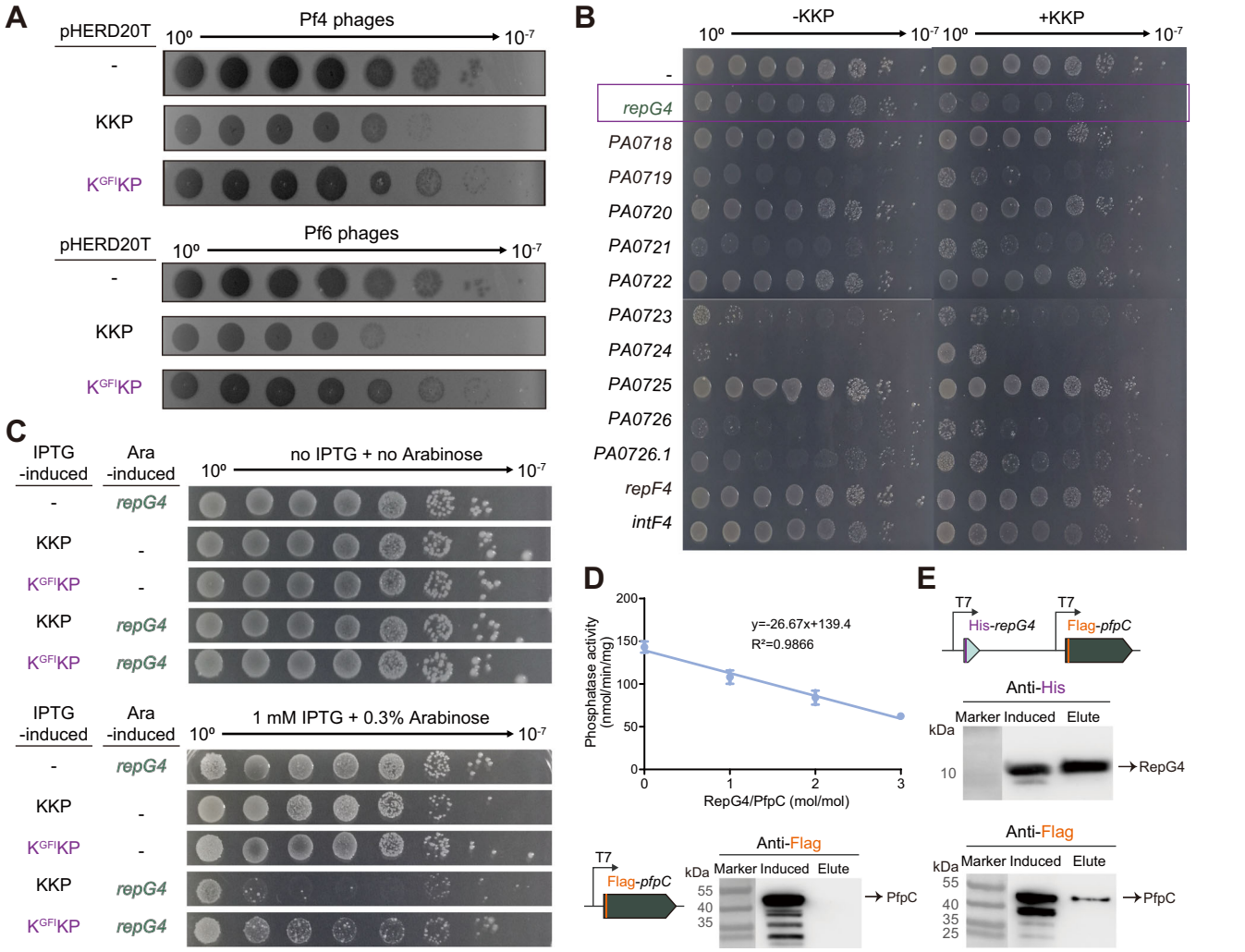

Fig. 4 | RepG4 activates the kinase-based toxicity of KKP. A Phage titers of Pf4 and Pf6 overexpressing pHERD20T, pHERD20T-KKP and pHERD20T-K^{GFI}KP were determined on ΔPf4ΔPf6 lawns. **B** Colony-forming units (CFUs) of KKP co-expressed with different Pf4-genes in MG1655 (+KKP). Pf4-genes in MG1655 (-KKP) were used as a control. KKP with *repG4* were boxed in purple. **C** CFU of KKP and K^{GFI}KP co-expressed with *repG4* in MG1655. **D** Phosphatase activity of PfpC in the presence or absence of RepG4. Three independent cultures were used, and data were shown as mean ± SD. **E** Pull-down assay between purified His-tagged RepG4 and Flag-tagged PfpC. Flag-tagged PfpC was shown as negative control. The term "Induced" denotes unpurified protein samples generated under induction conditions, whereas "Elute" refers to purified protein fractions obtained through imidazole-mediated elution from affinity chromatography matrices. The experiment in (**E**) was independently repeated twice, yielding similar results. Source data are provided as a Source Data file.

translational initiation in *repG6*, we cloned its native promoter region (~300 bp) and inserted an in-frame Flag-tag before the stop codon for detection. Site-directed mutagenesis (GTG → TGA) abolished protein production, confirming GTG as the functional start codon for *repG6* (Fig. 5C and Supplementary Fig. 8D). In contrast, *repG4* exclusively used its upstream ATG-mutagenesis (ATG → TGA) eliminated protein production, whereas modification of the GTG (GTG → TGA) only had minor effect, likely due to its interference with RBS (Fig. 5C and Supplementary Fig. 8D). Both proteins migrated at their predicted sizes (RepG4: ~8.5 kDa; RepG6: ~8.75 kDa) when expressed from their native regulatory elements (Supplementary Fig. 8D). These results demonstrate distinct translational initiation mechanisms between these homologous genes despite their conserved genomic contexts.

To elucidate the role of RepG4 in PfpC degradation, we incubated PfpC with lysates from MPAO1 cells overexpressing *repG* or from cells carrying an empty vector. RepG4 efficiently triggered PfpC proteolysis, whereas RepG6 suppressed PfpC proteolysis (Fig. 5D and Supplementary Fig. 8E, F), consistent with prior observations in Δ*pf4r* and Δ*pf6r* lysates (Fig. 5A). Structural prediction analysis identified four divergent residues between these two RepG homologs, including G26 (RepG4)/I27 (RepG6) in a loop region and R49 (RepG4)/C50 (RepG6) in an α-helix (Fig. 5E–G). Notably, mutating RepG4's R49 to C (mimicking RepG6) completely abolished its degradation activity while G26I mutant produced a phenotype identical to that of wild-type RepG4 (Fig. 5D and Supplementary Fig. 8F). Pull-down assays confirmed both RepG4 and RepG6 interact with Flag-tagged PfpC (Figs. 4E and 5H and Supplementary Fig. 8G), suggesting their opposing effects stem from post-binding regulation rather than binding affinity. Collectively, our findings demonstrate that the crosstalk between the core gene *repG4* of Pf4 and the accessory TA system of Pf6 coordinates the differential activation of these sister prophages during biofilm development. Moreover, we reveal that *repG6*, the core gene of Pf6, safeguards its own prophage functional elements through site-specific mutations. This interaction represents a sophisticated regulatory mechanism that balances phage propagation with host survival (Fig. 6 and Supplementary Fig. 9).

Discussion

Inoviruses are typically characterized by their small genomes and a unique chronic infection cycle, releasing progeny virions without

https://doi.org/10.1038/s41467-025-62378-6

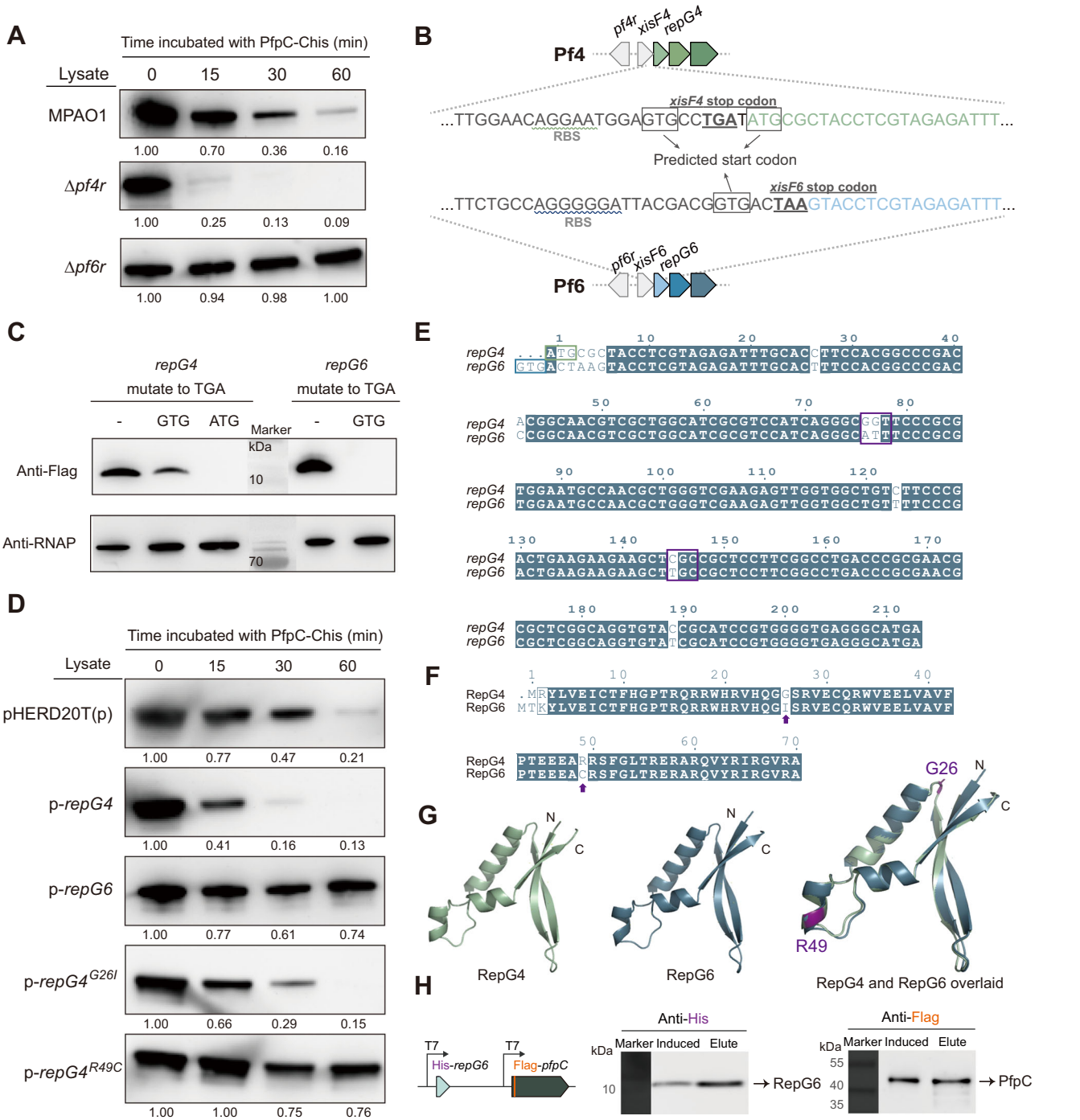

Fig. 5 | RepG4, but not RepG6, triggers PfpC degradation. A Quantification of the degradation of C-terminal His-tagged PfpC (~41 kDa) treated with MPAO1, Δ*pf4r* and Δ*pf6r* lysates for different times at 37 °C. The band retention percentage was calculated by ImageJ software (1.57f) and displayed below the corresponding band. The samples derive from the same experiment, and the blots were processed in parallel. **B** A schematic diagram indicates the intergenic region between excisionase XisF and RepG. The predicted start codons of *repG4* and *repG6* were boxed in gray. The predicted ribosome binding site (RBS) of RepG was lined in wavy. The stop codons of *xisF4* and *xisF6* were bolded. **C** Western blotting to determine the production of RepG4 and RepG6 using Flag antibody with pHERD20T-based constructs. **D** Quantification of the degradation of C-terminal His-tagged PfpC (~41 kDa) treated with MPAO1 overexpressing *repG* variants lysates for different times at 37 °C. The band retention percentage was calculated by ImageJ software (1.57f) and displayed below the corresponding band. The samples derive from the same experiment, and the blots were processed in parallel. Nucleotide sequences alignment (**E**), amino acid sequences alignment (**F**) and structure predicted by Alphafold2 (**G**) between *repG4* and *repG6*. Different residues inside the two homologs were highlighted in purple. **H** Pull-down assay between purified His-tagged RepG6 and Flag-tagged PfpC. Flag-tagged PfpC was shown as a negative control. The term "Induced" denotes unpurified protein samples generated under induction conditions, whereas "Elute" refers to purified protein fractions obtained through imidazole-mediated elution from affinity chromatography matrices. The experiments in (**A**, **C**, **D**, and **H**) were independently repeated twice, yielding similar results. Uncropped blots in Source Data.

https://doi.org/10.1038/s41467-025-62378-6

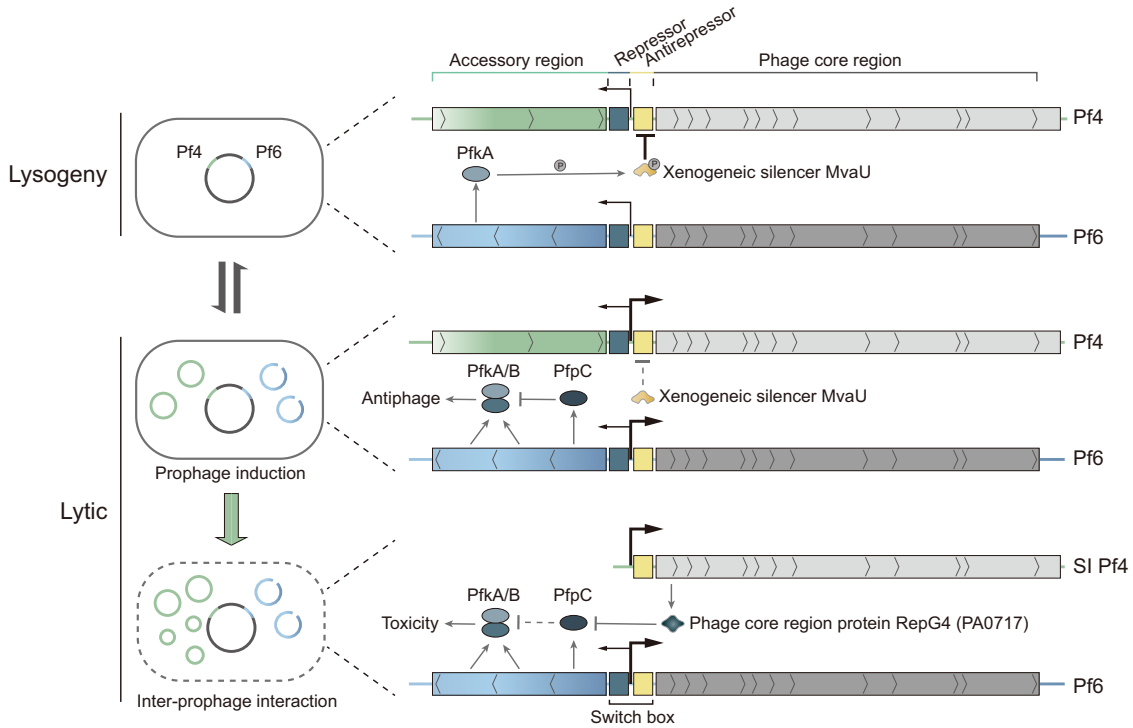

Fig. 6 | Model of the dynamic interplay between Pf4 and Pf6 in different host states. We previously found that in planktonic (free-living) cells, the kinase activity of the Pf6-encoded PfkA of the KKP TA module silences the Pf4 prophage in a lysogenic state by phosphorylating the host protein MvaU[6]. When the host switches to biofilm mode of growth, environmental cues/signaling pathways induce Pf6 activation, and the expression of PfpC increases, thereby dephosphorylating MvaU[6]. This results in Pf4 prophage excision and genome replication. Both Pf4 and Pf6 phages are synthesized and released as the biofilm develops, providing protection for host cells against antibiotics and dehydration. With further biofilm development, the Pf4-encoded reverse transcriptase (PfrT) synthesizes a reduced and SI Pf4 genome[38]. In the SI Pf4, XisF4 co-opts the promoter of the ncRNA to sustain high expression levels. In this study, we revealed that, if SI Pf4 reaches a very high level, RepG4 can trigger the degradation of PfpC, liberating the joint toxicity of PfkA-PfkB. The activation of the two kinases leads to host cell death to restrain further Pf phage production in a process similar to Abi. Thus, a balanced host: virus ratio is maintained.

causing host lysis[15,18]. However, studies of Pf phages in *P. aeruginosa* biofilms reveal a more complex life cycle, particularly in strains harboring multiple, related prophages. Building on previous findings[6,13,38], we demonstrate a dynamic interplay between Pf4 and Pf6 prophages in *P. aeruginosa* under different growth conditions (Fig. 6 and Supplementary Fig. 9). In planktonic cells, the Pf4 antirepressor/excisionase gene (*xisF4*), regulated by host silencers MvaU/MvaT, prevents Pf4 activation[6]. The Pf6-encoded PfkA kinase, part of the KKP TA module, maintains Pf4 lysogeny by phosphorylating MvaU[6]. Biofilm formation and associated stresses activate Pf6, upregulating *pfpC* expression, which dephosphorylates MvaU, triggering Pf4 excision and replication[6]. We recently reported that Pf4 phages released late in biofilm development lose approximately one-quarter of their genome, retaining only core genes; this process is regulated by the Pf4-encoded reverse transcriptase PfrT[38]. This genome reduction eliminates repressor binding sites, converting non-SI Pf4 to SI Pf4, enabling re-infection and host cell death[38].

This study demonstrates that the core Pf4 protein RepG4 promotes PfpC degradation, thereby unleashing the toxic activity of the PfkA-PfkB kinase complex. This cascade induces host cell death and restricts phage propagation, resembling an abortive infection mechanism. Bioinformatics analyses suggest RepG homologs in Pf1 and Pf5 may similarly activate KKP-mediated toxicity, whereas RepG6 (the Pf6 counterpart) appears to stabilize PfpC. This dichotomous regulation may enable discrimination between "self" (Pf6) and "non-self" (Pf4/Pf1/Pf5) prophages in terms of KKP regulation during prophage activation. Despite these antagonistic interactions, the system ultimately maintains a symbiotic relationship that enhances bacterial fitness and virulence. Through mechanisms including biofilm formation and immune evasion[8], this phage-host interplay demonstrates a complicated co-evolutionary adaptation where accessory prophage genes confer mutual benefits to both phage and bacterial host.

Despite sharing a highly similar core region, Pf4 and Pf6 employ distinct replication strategies upon activation. Pf4 utilizes an RCR mechanism, followed by prophage excision to generate circular, non-SI genomes containing the full-length Pf4 prophage genome[19,46]. Similar to CTXφ phages[47,48], Pf4 and CTXφ replication rely on an initiator protein (RepF4 and RstA, respectively) and the host-encoded UvrD helicase, typically involved in DNA repair[46,48]. In contrast to Pf4, Pf6 activation appears to follow a distinct replication strategy. Although Pf6 activation requires RepF6, we detected only minimal circularized genomes and no significant increase in prophage excision during biofilm-associated activation. Unlike XisF4, overexpression of XisF6 failed to induce either prophage excision or Pf6 activation, suggesting that Pf6 may replicate without relying on genome excision in biofilms. Furthermore, we found previously that the Pf4-encoded reverse transcriptase gene, *pfrT*, is involved in the synthesis of SI Pf4 phages and Pf6 phages during biofilm formation[38]. Further investigation is needed to elucidate the precise replication mechanism of Pf6 prophage in biofilm.

Prophages frequently harbor numerous antiphage defense elements, shown previously to provide protection against lytic phage infection[6,49–52]. These defense systems, often located within the prophage accessory genome, are expressed even in the lysogenic state[51]. They can act as repressors of cognate prophages and defend against competing lytic phages, thereby promoting host growth and survival[50]. Under stress conditions, such as those associated with

biofilm growth that can trigger prophage activation, these prophage-encoded defense systems monitor prophage induction levels, interacting with genes involved in phage replication and assembly to prevent rapid phage virion proliferation[6]. Our study reveals a critical surveillance mechanism involving key phage proteins and accessory phage-encoded defense systems, coordinating phage-phage and host-phage interactions in polylysogenic bacteria. The function of these Pf-encoded defense systems in regulating prophage induction within eukaryotic hosts warrants further investigation.

Methods

Bacterial strains, plasmids, and growth conditions

The bacterial strains, plasmids and all primers used in this study are listed in Supplementary data 1 and Supplementary data 2 in Supplementary file. The *E. coli* and *P. aeruginosa* MPAO1 wild-type and mutant strains were grown in LB medium (Bertani, 1951), at 37 °C except where indicated. Carbenicillin (100 μg/mL) was used to maintain pHERD20T-based plasmids and pEX18Ap-based plasmids, chloramphenicol (30 μg/mL) was used to maintain pTac-based plasmids and gentamycin (30 μg/mL) was used to maintain pEX18Gm-based plasmids, which were used to delete genes in MPAO1. 0.3% (w/v) *L*-arabinose was used to induce the expression of target genes in pHERD20T-based plasmids. 1 mM IPTG (isopropyl-β-D-thiogalactopyranoside) was used to induce the expression of target genes in pTac-based plasmids.

Deletion of genes in the MPAO1 chromosome

The mutant strains were generated using a rapid method for the generation of *P. aeruginosa* deletion mutants with modifications[53]. Considering the co-transcription of *PA0717-PA0718-PA0719*, we only mutated the start codon of each gene and inserted a gentamycin sequence. Fragments were ligated into pEX18Gm/pEX18Ap plasmid digested with EcoRI and HindIII using one-step ligation kit (Vazyme Biotechnology Corporation, Nanjing, China). Then the ligated products were transferred into the diaminopimelic acid (DAP) auxotrophic RP4 conjugal donor *E. coli* strain WM3064. The correct constructs were confirmed by both PCR and sequencing. Then they were conjugated into MPAO1 cells. Following this, the in-frame deletion mutants were generated via homologous recombination using the sucrose resistance selection method. The mutations were verified using PCR and DNA sequencing with the gene-LF/LR primer pair.

Biofilm growth and sample collection

A flow cell biofilm system cultured in M9 medium (47.8 mM Na_2HPO_4, 22 mM KH_2PO_4, 6.8 mM NH_4Cl, 18.7 mM NaCl, 100 μM $CaCl_2$, 2 mM $MgSO_4$ and 0.1% glucose) was conducted as previously described with minor modification[6]. In details, 1 mL of fresh overnight cultures was injected into the inlet of medical silicone catheters (with an inner diameter of 3 mm and a length of 400 mm, produced by Forbest Manufacturing Corporation, Shenzhen, China), taking care to prevent bubble formation. Subsequently, the inoculated catheters were left static for 1 h to facilitate colonization of the bacteria on the inner surface of the catheters. After this colonization period, a peristaltic pump was used to initiate flow at a rate of 0.1 mL per minute for each channel. At specific time points, phages were collected from the effluents, and biofilm cells inside the catheters were obtained by cutting the catheters open. During the experiment, fresh M9 medium was supplied daily, and the total assay runtime varied between 4 and 6 days, depending on the specific readout requirements. Phages in biofilm effluents were collected on mentioned days by collecting 2 mL of newly flowed M9 culture. Subsequently, the collected effluents were filtered through a 0.22-μm pore size filter (Millipore) and treated with 1 μg mL^{-1} DNase I (New England Biolabs, MA, USA) at room temperature for 1.5 h and stored at 4 °C[54]. Biofilm cells in the inner surface of the medical catheter were collected by cutting 1 cm section and stored at −80 °C.

Quantification of Pf4 and Pf6 phages in effluents

Total phage titers in the effluents were quantified using the traditional top-layer agar method[55]. In brief, the treated effluents were serially diluted 10-fold in SM buffer, and a volume of 5 μL medium of each dilution was spotted on R-top layer media supplemented with the MPAO1 wild-type or ΔPf4ΔPf6 strains. Then the agar plates were incubated at 37 °C for 16 h. After that, the phage-forming units in biofilm effluents were calculated by multiplying the number of countable plaques on agar plates by the dilution fold and then by 200. The ratio between Pf4 and Pf6 phages in biofilm effluents was determined using a qPCR assay.

Quantitative PCR (qPCR) assay

The quantification of Pf4 and Pf6 genes in biofilms and planktonic cells was determined using a qPCR-based method we established previously[6]. For the quantification of Pf phages, a volume of 1 μL stored effluent was treated with DNase I and then used as a PCR template, and the MPAO1 chromosome-specific gene *gyrB* was used as a negative control to exclude contamination of host genomic DNA. For the biofilms and planktonic cells, genomic DNA was isolated using a TIANamp Bacteria DNA Kit (Tiangen Biotech Co., Ltd., Beijing, China) following the manufacturer's instructions. During the DNA isolation process, RNA was removed by adding 10 U/μL RNase A during cell lysis. A total of 20 ng of DNA from each sample was utilized to quantify the copy numbers of Pf genes. The fold change of Pf4 and Pf6 in each effluent/cell sample was calculated based on their specific genes listed in Supplementary data 2. For Pf4 phages, specific Pf4 primers (Pf4-*attB*, Pf4-*attP*, *xisF4*, *pfiA*, and *repF4*) were used, which are not present in Pf6. For Pf6 phages, specific Pf6 primers (Pf6-*attB*, Pf6-*attP*, *intF6*, *pfkA*, and *repF6*) were used, which are not present in Pf4.

Copy numbers of Pf4 and Pf6 phages in biofilm cells

Total genomic DNA was isolated from biofilm cells using a TIANamp Bacteria DNA Kit (Tiangen Biotech Co., Ltd., Beijing, China) following the manufacturer's instructions. To exclude RNA contamination, the potential RNA was removed by adding 10 U $μl^{-1}$ of RNase for 20 min at room temperature during the DNA isolation process. Then 20 ng DNA of each sample was used as template. In addition to *pfiA* and *intF6*, Pf4-*attP* was used to determine the copy number of Pf4 and Pf6-*attP* was used to determine the copy number of Pf6 in the same cells.

Co-expression toxicity assay

Co-expression of KKP was performed using two-plasmid system with pTac and pHERD20T promoters. For measurements of colony-forming units (CFU), overnight cells were diluted to an OD600 ≈of 0.1, and cells were cultured for 6 h in LB medium with 0.1 mg mL^{-1} carbenicillin and 0.03 mg mL^{-1} chloramphenicol, followed by being diluted serially and dropped onto the plate with 1mM IPTG and 0.3% *L*-arabinose. Plates with 0.1 mg mL^{-1} carbenicillin and 0.03 mg mL^{-1} chloramphenicol were used as a control. Then, plates were incubated at 37 °C for 16 h.

Whole-genome sequencing of phages and resequencing of hosts

The experiments were conducted strictly following our previous study[38]. In brief, whole bacterial genomic DNA and whole ssDNA genome of Pf phages in biofilm cells and effluents were isolated using a TIANamp Bacteria DNA Kit and a TIANamp Virus DNA/RNA Kit (Tiangen, Beijing, China). Then the following double-stranded DNA generating from ssDNA, DNA library construction and sequencing are carried out in GENEWIZ (Suzhou, China).

Plaque assay

Pf phages released from biofilms as reported previously were collected at mentioned days[56,57]. A total of 1 mL of culture was centrifuged, and

the supernatant was filtered through a 0.22-μm filter (Millipore Millex GP) to obtain the Pf phage solution. The filtered Pf phage was serially diluted with LB, and 5 μL was dropped onto bacterial lawns. For the overexpression strains, the overnight cultures were diluted to OD = 0.1 and cultured for 2 h, then *L*-arabinose was added to induce the expression of genes for 4 h. The double-layer agar plates for the plaque assay were prepared as reported previously[37].

Protein 3D structure prediction

Structure of Pf6r (PDB ID: 6X6F) was based on the crystal structure in PDB. The tertiary structures of RepF4, RepF6, XisF4, XisF6, Pf4r, RepG4 and RepG6 were predicted with AlphaFold2 (https://alphafold.com/)[58]. For structural alignment, structural figures were produced with PyMOL (www.pymol.org).

Comparison of Pf phages

The Pf phages from different strains were compared by tBLASTx using program Easyfig_2.2.5_win[59]. In brief, the amino acid sequences of different Pf phages were downloaded from NCBI in GenBank format, followed by uploading to Easyfig_2.2.5_win and being aligned with tBLASTx.

Protein purifications

A 500 mL LB medium containing the indicated antibiotic was inoculated with 3 mL overnight pre-culture and grown at 37 °C with shaking (200 rpm). Inducer was added from $OD_{600} \approx 0.5$ and culture were incubated at 37 °C for 16 h. Overnight cell pellets were collected by centrifugation (4500 × *g* for 30min) and resuspended using Buffer A (500 mM NaCl, 40 mM Tris-HCl, 10 mM imidazole, pH 8.0), followed by being lysed via ultrasonication, and the supernatant was collected. Ni-NTA resin was used to bind the His-tagged protein, and proteins were eluted with increasing concentrations of imidazole. The eluted proteins were collected, dialyzed against buffer (200 mM NaCl, 20 mM Tris-HCl, pH 8.0) and stored on ice.

Protein degradation assays

Purified proteins were incubated with the cell lysates for the indicated times at 37 °C/4 °C. In detail, overnight cultures were diluted to $OD_{600} \approx 0.1$ and cultured for 8 h. Then, the cell pellets were collected; for overexpression cells, the overnight cultures were diluted to $OD_{600} \approx 0.1$ and cultured for 4 h and then *L*-arabinose was added to induce target gene expression for 4 h. The cell pellets were resuspended in lysis buffer (200 mM NaCl, 20 mM Tris-HCl, pH 8.0), followed by ultrasonication and centrifugation to collect the supernatant. Equal-volume aliquots of the lysate were then co-incubated with 0.1 μg/μL PfpC for 0, 15, 30, and 60 min at 37 °C, followed by western blotting.

Western blotting

Proteins were separated on Tricine gels, transferred to PVDF membranes (Millipore), and blocked with Fast Blocking Buffer (Yeasen, #36122ES60, China). The membranes were incubated with primary antibodies (His Tag Mouse Monoclonal Antibody, #AF2876, 1:3000, Beyotime; Flag Tag Mouse Monoclonal Antibody, #AF2852, 1:3000, Beyotime; RNA polymerase beta Antibody, #T57097M, 1:3000, Abmart) at 4 °C overnight. After washing with 1 × TBST (diluted from 10 × TBST, Yeasen #60145ES76), the membranes were probed with Secondary Antibody (HRP-conjugated goat anti-mouse IgG(H + L), #A0216; 1:3000, Beyotime; HRP-conjugated goat anti-rabbit IgG(H + L), #A0208, 1:3000, Beyotime) for 1 h at room temperature. Signals were detected using an imaging system (Tanon 5200, China) and the band retention percentage was calculated by ImageJ software (1.57f) and displayed below the corresponding band.

Phosphatase activity assay

The phosphatase activity of PfpC was determined using the Beyotime Alkaline Phosphatase Assay Kit (Nanjing, China) following the manufacturer's instructions. Purified PfpC was premixed with different concentrations of PA0717 and incubated on ice for 30 min to allow the formation of the complex. The reaction system includes 10 μL of 0.5 μg/μL PfpC (molar mass ~12 μM) as the fixed component, supplemented with 1:1, 1:2, and 1:3 molar ratios of PA0717 (0.1 μg/μL; molar mass ~12 μM). Then, the substrates were added into the reaction system and incubated at 37 °C for 5 min. PfpC phosphatase activity was expressed as nmol min^{-1} mg^{-1} protein. Enzymatic activity was measured three times with the same sample.

Pull-down assay

Flag-tagged PfpC was cloned into pETDuet digested with NdeI and XhoI to construct pETDuet-*flag-pfpC*, and it was then digested by NcoI and HindIII. Next, N-terminal 6xHis-tagged *repG4* was introduced to obtain pETDuet-His- *repG4*-Flag-*PfpC*. The plasmid was transformed into *E. coli* strain Rosetta cells, and the cells were cultured at 37 °C. The overexpression was induced by 0.5 mM IPTG at 16 °C for 12 h when the OD_{600} value reached 0.6–0.8. Then, the pull-downs with the cloned genes were performed. Briefly, pellets were collected by centrifugation at 4500 × *g* for 30 min at 4 °C. The cell pellet was resuspended using Buffer A (250 mM NaCl, 40 mM Tris-HCl, 10 mM imidazole, pH 8.0) and lysed via ultrasonication, and the supernatant was collected. Ni-NTA resin was used to bind the His-tagged protein, and proteins were eluted with increasing concentrations of imidazole. Rosetta/pETDuet-*flag-pfpC* was included as a control. The Elute were then subjected to Tricine-SDS PAGE and Western blotting using anti-His and anti-Flag tag antibodies.

Statistics and reproducibility

For all experiments, at least three independent biological replicates were used unless otherwise noted. The experiments were independently repeated twice, yielding similar results. Significance testing was performed by an unpaired T-test for comparisons between two groups, and a one-way analysis of variance (ANOVA) test with Tukey's correction for multiple comparisons. A p-value of <0.05 was considered statistically significant.

Reporting summary

Further information on research design is available in the Nature Portfolio Reporting Summary linked to this article.

Data availability

The data that support the findings of this study are provided within the manuscript and its associated Supplementary Information. The raw data for deep sequencing of phages and biofilm cells have been deposited in the Sequence Read Archive (SRA) under BioProject accession number PRJNA1113957. The raw transcriptomic data supporting this study were deposited in GEO under accession number GSE299861 and have been described in our prior work[6]. The mass spectrometry proteomics data have been deposited to the ProteomeXchange (http://proteomecentral.proteomexchange.org) via the PRIDE partner repository Project accession: PXD059573. Source data are provided with this paper. There are no restrictions on data availability. Source data are provided with this paper.

References

1. Feiner, R. et al. A new perspective on lysogeny: prophages as active regulatory switches of bacteria. *Nat. Rev. Microbiol.* **13**, 641–650 (2015).
2. Perna, N. T. et al. Genome sequence of enterohaemorrhagic *Escherichia coli* O157:H7. *Nature* **409**, 529–533 (2001).
3. Ochman, H. et al. The defective prophage pool of *Escherichia coli* O157: prophage–prophage interactions potentiate horizontal transfer of virulence determinants. *PLoS Pathog.* **5**, e1000408 (2009).

4. Lemire, S., Figueroa-Bossi, N. & Bossi, L. Bacteriophage crosstalk: coordination of prophage induction by trans-acting antirepressors. *PLoS Genet*. **7**, e1002149 (2011).
5. Figueroa-Bossi, N., Uzzau, S., Maloriol, D. & Bossi, L. Variable assortment of prophages provides a transferable repertoire of pathogenic determinants in *Salmonella*. *Mol. Microbiol.* **39**, 260–272 (2001).
6. Guo, Y. et al. Control of lysogeny and antiphage defense by a prophage-encoded kinase-phosphatase module. *Nat. Commun.* **15**, 7244 (2024).
7. Argov, T. et al. Coordination of cohabiting phage elements supports bacteria–phage cooperation. *Nat. Commun.* **10**, 5288 (2019).
8. Howard-Varona, C., Hargreaves, K. R., Abedon, S. T. & Sullivan, M. B. Lysogeny in nature: mechanisms, impact and ecology of temperate phages. *ISME J.* **11**, 1511–1520 (2017).
9. Silpe, J. E., Duddy, O. P. & Bassler, B. L. Induction mechanisms and strategies underlying interprophage competition during polylysogeny. *PLOS Pathog.* **19**, e1011363 (2023).
10. Pfeifer, E., Sousa, J. M., Touchon, M. & Rocha, E. P. When bacteria are phage playgrounds: interactions between viruses, cells, and mobile genetic elements. *Curr. Opin. Microbiol.* **70**, 102230 (2022).
11. Refardt, D. Within-host competition determines reproductive success of temperate bacteriophages. *ISME J.* **5**, 1451–1460 (2011).
12. Ismail, M. H. et al. The repressor C protein, Pf4r, controls superinfection of *Pseudomonas aeruginosa* PAO1 by the Pf4 filamentous phage and regulates host gene expression. *Viruses* **13**, 1614 (2021).
13. Li, Y. et al. Excisionase in Pf filamentous prophage controls lysis-lysogeny decision-making in *Pseudomonas aeruginosa*. *Mol. Microbiol.* **111**, 495–513 (2019).
14. Silpe, J. E. et al. Small protein modules dictate prophage fates during polylysogeny. *Nature* **620**, 625–633 (2023).
15. Roux, S. et al. Cryptic inoviruses revealed as pervasive in bacteria and archaea across Earth's biomes. *Nat. Microbiol.* **4**, 1895–1906 (2019).
16. Waldor, M. K. & Mekalanos, J. J. Lysogenic conversion by a filamentous phage encoding cholera toxin. *Science* **272**, 1910–1914 (1996).
17. Rice, S. A. et al. The biofilm life cycle and virulence of *Pseudomonas aeruginosa* are dependent on a filamentous prophage. *ISME J.* **3**, 271–282 (2009).
18. Hay, I. D. & Lithgow, T. Filamentous phages: masters of a microbial sharing economy. *EMBO Rep.* **20**, e47427 (2019).
19. Secor, P. R. et al. Pf bacteriophage and their impact on *Pseudomonas* virulence, mammalian immunity, and chronic infections. *Front. Immunol.* **11**, 244 (2020).
20. Bondy-Denomy, J. & Davidson, A. R. When a virus is not a parasite: the beneficial effects of prophages on bacterial fitness. *J. Microbiol.* **52**, 235–242 (2014).
21. Brouwer, S. et al. Prophage exotoxins enhance colonization fitness in epidemic scarlet fever-causing *Streptococcus pyogenes*. *Nat. Commun.* **11**, 5018 (2020).
22. Rousset, F. et al. Phages and their satellites encode hotspots of antiviral systems. *Cell Host Microbe* **30**, 740–753 (2022).
23. Kita, K. et al. Evidence of horizontal transfer of the Eco O109I restriction-modification gene to *Escherichia coli* chromosomal DNA. *J. Bacteriol.* **181**, 6822–6827 (1999).
24. Jurenas, D., Fraikin, N., Goormaghtigh, F. & Van Melderen, L. Biology and evolution of bacterial toxin-antitoxin systems. *Nat. Rev. Microbiol.* **20**, 335–350 (2022).
25. Kelly, A., Arrowsmith, T. J., Went, S. C. & Blower, T. R. Toxin–antitoxin systems as mediators of phage defence and the implications for abortive infection. *Curr. Opin. Microbiol.* **73**, 102293 (2023).
26. Leroux, M. & Laub, M. T. Toxin-antitoxin systems as phage defense elements. *Ann. Rev. Microbiol* **76**, 21–43 (2022).
27. Pinilla-Redondo, R. et al. Discovery of multiple anti-CRISPRs highlights anti-defense gene clustering in mobile genetic elements. *Nat. Commun.* **11**, 5652 (2020).
28. Zhang et al. Direct activation of a bacterial innate immune system by a viral capsid protein. *Nature* **612**, 132–140 (2022).
29. Zhang, T. et al. A bacterial immunity protein directly senses two disparate phage proteins. *Nature* **635**, 728–735 (2024).
30. Uc-Mass, A. et al. An orthologue of the cor gene is involved in the exclusion of temperate lambdoid phages. Evidence that Cor inactivates FhuA receptor functions. *Virology* **329**, 425–433 (2004).
31. Jacobs, M. A. et al. Comprehensive transposon mutant library of *Pseudomonas aeruginosa*. *Proc. Nat. Acad. Sci.* **100**, 14339–14344 (2003).
32. Klockgether, J. et al. Genome diversity of *Pseudomonas aeruginosa* PAO1 laboratory strains. *J. Bacteriol.* **192**, 1113–1121 (2010).
33. Webb, J. S., Lau, M. & Kjelleberg, S. Bacteriophage and phenotypic variation in *Pseudomonas aeruginosa* biofilm development. *J. Bacteriol.* **186**, 8066–8073 (2004).
34. Webb, J. S. et al. Cell death in *Pseudomonas aeruginosa* biofilm development. *J. Bacteriol.* **185**, 4585–4592 (2003).
35. Whiteley, M. et al. Gene expression in *Pseudomonas aeruginosa* biofilms. *Nature* **413**, 860–864 (2001).
36. Sweere, J. M. et al. Bacteriophage trigger antiviral immunity and prevent clearance of bacterial infection. *Science* **363**, eaat9691 (2019).
37. Li, Y. et al. Prophage encoding toxin/antitoxin system PfiT/PfiA inhibits Pf4 production in *Pseudomonas aeruginosa*. *Microb. Biotechnol.* **13**, 1132–1144 (2020).
38. Guo, Y. et al. A reverse transcriptase controls prophage genome reduction to promote phage dissemination in *Pseudomonas aeruginosa* biofilms. *Cell Rep.* **43**, 114883 (2024).
39. Wang, W. et al. Filamentous prophage capsid proteins contribute to superinfection exclusion and phage defence in *Pseudomonas aeruginosa*. *Environ. Microbiol.* **24**, 4285–4298 (2022).
40. Schmidt, A. K. et al. A filamentous bacteriophage protein inhibits type IV pili to prevent superinfection of *Pseudomonas aeruginosa*. *Mbio* **13**, e0244121 (2022).
41. Ilyina, T. V. & Koonin, E. V. Conserved sequence motifs in the initiator proteins for rolling circle DNA replication encoded by diverse replicons from eubacteria, eucaryotes and archaebacteria. *Nucleic Acids Res.* **20**, 3279–3285 (1992).
42. Ronning, D. R. et al. Active site sharing and subterminal hairpin recognition in a new class of DNA transposases. *Mol. Cell* **20**, 143–154 (2005).
43. Schmidt, A. K. et al. Targeted deletion of Pf prophages from diverse *Pseudomonas aeruginosa* isolates has differential impacts on quorum sensing and virulence traits. *J. Bacteriol.* **206**, e0040223 (2024).
44. Xiong, L. et al. Arginine metabolism in bacterial pathogenesis and cancer therapy. *Int. J. Mol. Sci.* **17**, 363 (2016).
45. Weng, J., Guo, Y., Gu, J., Chen, R. & Wang, X. Inovirus-encoded peptides induce specific toxicity in *Pseudomonas aeruginosa*. *Viruses* **17**, 112 (2025).
46. Martínez, E. & Campos-Gómez, J. Pf filamentous phage requires UvrD for replication in *Pseudomonas aeruginosa*. *mSphere* **1**, e00104–e00115 (2016).
47. Moyer, K. E., Kimsey, H. H. & Waldor, M. K. Evidence for a rolling-circle mechanism of phage DNA synthesis from both replicative and integrated forms of CTXφ. *Mol. Microbiol.* **41**, 311–323 (2001).
48. Martínez, E., Paly, E. & Barre, F. X. CTXφ Replication Depends on the Histone-Like HU Protein and the UvrD Helicase. *PLOS Genet.* **11**, e1005256 (2015).

49. Sargen, M. R. & Helaine, S. A prophage competition element protects *Salmonella* from lysis. *Cell Host Microbe* **32**, 2063–2079 (2024).
50. Owen, S. V. et al. Prophages encode phage-defense systems with cognate self-immunity. *Cell Host Microbe* **29**, 1620–1633.e1628 (2021).
51. Georjon, H. & Bernheim, A. The highly diverse antiphage defence systems of bacteria. *Nat. Rev. Microbiol.* **21**, 686–700 (2023).
52. Dedrick, R. M. et al. Prophage-mediated defence against viral attack and viral counter-defence. *Nat. Microbiol.* **2**, 16251 (2017).
53. Choi, K. H. & Schweizer, H. P. An improved method for rapid generation of unmarked *Pseudomonas aeruginosa* deletion mutants. *BMC Microbiol* **5**, 30 (2005).
54. McElroy, K. E. et al. Strain-specific parallel evolution drives short-term diversification during *Pseudomonas aeruginosa* biofilm formation. *Proc. Nat. Acad. Sci.USA* **111**, E1419–E1427 (2014).
55. Hershey, A. D., Kalmanson, G. & Bronfenbrenner, J. Quantitative methods in the study of the phage-antiphage reaction. *J. Immunol.* **46**, 267–279 (1943).
56. Woo, J. K., Webb, J. S., Kirov, S. M., Kjelleberg, S. & Rice, S. A. Biofilm dispersal cells of a cystic fibrosis *Pseudomonas aeruginosa* isolate exhibit variability in functional traits likely to contribute to persistent infection. *FEMS Immunol. Med. Microbiol.* **66**, 251–264 (2012).
57. Barraud, N. et al. Nitric oxide signaling in *Pseudomonas aeruginosa* biofilms mediates phosphodiesterase activity, decreased cyclic di-GMP levels, and enhanced dispersal. *J. Bacteriol.* **191**, 7333–7342 (2009).
58. Jumper, J. et al. Highly accurate protein structure prediction with AlphaFold. *Nature* **596**, 583–589 (2021).
59. Sullivan, M. J., Petty, N. K. & Beatson, S. A. Easyfig: a genome comparison visualizer. *Bioinformatics* **27**, 1009–1010 (2011).
60. Malgaonkar, A. & Nair, M. Quorum sensing in *Pseudomonas aeruginosa* mediated by RhlR is regulated by a small RNA PhrD. *Sci. Rep.* **9**, 432 (2019).
61. Wei, Q. et al. Global regulation of gene expression by OxyR in an important human opportunistic pathogen. *Nucleic Acids Res.* **40**, 4320–4333 (2012).
62. Schwartzkopf, C. M. et al. Inhibition of PQS signaling by the Pf bacteriophage protein PfsE enhances viral replication in *Pseudomonas aeruginosa*. *Mol. Microbiol.* **121**, 116–128 (2024).

Acknowledgements

This work was supported by the Ocean Negative Carbon Emissions (ONCE) Program, National Science Foundation of China (42188102 to X.X.W., 32470032 to Y.X.G. and 92451302 to Y.X.G.), by the Science & Technology Fundamental Resources Investigation Program (2022FY100600 to X.X.W.), by the National Science Foundation of Guangdong Province (2024A1515011146 to Y.X.G.), by the Guangdong Major Project of Basic and Applied Basic Research (2019B030302004 to Y.X.G.), by the Guangdong Local Innovation Team Program (2019BT02Y262 to X.X.W. and Y.X.G.), by the special fund of South China Sea Institute of Oceanology of the Chinese Academy of Sciences (SCSIO2023QY03 to X.X.W.).

Author contributions

X.X.W. and J.Y.G. conceived the project. J.Y.G. and Y.X.G. performed the experiments and data analysis. J.H.W., S.T.L., and Y.B.L. assisted with experimental procedures and data analysis. All authors interpreted the data. X.X.W. and J.Y.G. wrote the manuscript.

Competing interests

The authors declare no competing interests.

Additional information

Supplementary information The online version contains supplementary material available at https://doi.org/10.1038/s41467-025-62378-6.

Correspondence and requests for materials should be addressed to Xiaoxue Wang.

Peer review information *Nature Communications* thanks the anonymous reviewers for their contribution to the peer review of this work. A peer review file is available.